Preparation, characterization and environmental/electrochemical energy storage testing of low-cost biochar from natural chitin obtained via pyrolysis at mild conditions

UNIVERSITÀ DEGLI STUDI DI TORINO

Preparation, characterization and environmental/electrochemical energy storage testing of low-cost biochar from natural chitin obtained via pyrolysis at mild conditions

Giuliana Magnacca[a,b], Federico Guerretta[a], Alen Vizintin[c], Paola Benzi[a], Maria C. Valsania[a], Roberto Nisticò[a,d,*]

[a] University of Torino, Department of Chemistry, Via P. Giuria 7, 10125 Torino, Italy
[b] NIS Interdepartmental Centre, Via P. Giuria 7, 10125 Torino, Italy
[c] Department of Materials Chemistry, National Institute of Chemistry, Hajdrihova 19, 1000 Ljubljana, Slovenia
[d] Polytechnic of Torino, Department of Applied Science and Technology DISAT, C.so Duca degli Abruzzi 24, 10129 Torino, Italy

A B S T R A C T

Chitin (a biopolymer obtained from shellfish industry) was used as precursor for the production of biochars obtained via pyrolysis treatments performed at mild conditions (in the 290–540 °C range). Biochars were physicochemical characterized in order to evaluate the pyrolysis-induced effects in terms of both functional groups and material structure. Moreover, such carbonaceous materials were tested as adsorbent substrates for the removal of target molecules from aqueous environment as well as in solid-gas experiments, to measure the adsorption capacities and selectivity toward CO_2. Lastly, biochars were also investigated as possible cathode materials in sustainable and low-cost electrochemical energy storage devices, such as lithium-sulphur (Li-S) batteries. Interestingly, experimental results evidenced that such chitin-derived biochars obtained via pyrolysis at mild conditions are sustainable, low-cost and easy scalable alternative materials suitable for both environmental and energetic applications.

1. Introduction

The term "biochar" initially referred to a "carbon-rich product obtained when biomasses (i.e., wood, manure or leaves) are heated in a closed container with little or no available air" [1]. Actually, the official definition of biochar as a "solid material produced by the thermal decomposition of biomasses under limited supply of oxygen, and at relatively low temperatures (i.e., below 700 °C)" was provided by the International Biochar Initiative (IBI) [2]. Since the process used for obtaining biochar often mirrors the industrial production of charcoal, it is mandatory to provide a clarification. In particular, basing on the latter definition, the biochar category can be extended also to all carbonaceous materials obtained from raw materials and/or substances not directly related to the agriculture and wood industry. Moreover, it is possible to clearly distinguish a biochar (a carbonaceous material produced with the intent to be applied in soils, and, in a broader sense, for environmental applications) from a charcoal (a carbonaceous material produced with the intent to be applied as fuel in energetic fields) on the basis of their final application [2,3]. In all cases, biochar is produced by a single pyrolysis treatment performed directly on solid precursors under inert (absence/limited supply of oxygen) atmosphere.

According to the literature [4], carbon-based materials are the most versatile substrates that can be used in both environmental and electrochemical applications. Among the different standard carbonaceous materials, carbon nanotubes (CNTs) and graphene (i.e., a single-atom thick planar sheet of carbon atoms organized in a honeycomb fashion) represent very interesting nanostructured substrates, and since from their discoveries several studies are involved in the exploitation of these promising nanomaterials in several technological fields [5–7], ranging from the environmental remediation of contaminated wastewater, in gas separation/storage, catalysis, batteries and other energetic applications, and many others. In detail, CNTs are extensively studied as attractive adsorbing materials for the removal of (in)organic pollutants from contaminated wastewater due to their high surface area [5], whereas, several studies reported that both the chemical and electronic performances of such graphene and CNTs can be modified by introducing nitrogen heteroatoms in the chemical structure

* Corresponding author at: Polytechnic of Torino, Department of Applied Science and Technology DISAT, C.so Duca degli Abruzzi 24, Torino, 10129, Italy.
E-mail address: roberto.nistico@polito.it (R. Nisticò).

[6,7]. Quite recently, there is a growing interest around the valorization of low-cost biopolymers obtained from natural sources as possible sustainable/cheap precursors for the production of carbon-rich materials [4,8–13]. Considering this interest, the present paper faces the possibility of using chitin as carbon precursor.

Chitin is one of the most abundant natural biopolymer obtained mainly from the external shells of crustaceans (crabs, shrimps, lobsters), as well as from radulae, beaks and cuttlebones of cephalopods (squid and octopuses), therefore it can be assumed as a shellfish industry biowaste [14–16]. From the chemical viewpoint, chitin is a β (1–4) glycan, formed by 2-acetamide-2-deoxy-D-glucopyranose units, randomly N-deacetylated (DD below 50%) [17]. Unfortunately, the utilization/processability of chitin is quite limited by its insolubility in many common solvents [16]. In order to overcome this significant limitation, chitin is preferentially converted into the much more soluble chitosan (the corresponding N-deacetylated form) [16,18], which found applications in several technologic fields, mainly in water remediation as adsorbent or in biomedicine as drug carrier/antimicrobial agent [19–27].

In our recent study focused on the pyrolysis behavior of chitin/chitosan [17], the degradation pattern of both biopolymers was unveiled, revealing the formation of N-containing heteroaromatic species as well as a significant carbonaceous residue, thus pointing out the possibility of using such aminopolysaccharides as precursors for the production of N-doped carbon-based materials [28].

Actually, several studies report the use of chitin as sustainable carbon precursor [28–37]. In many works, carbonization was carried out by means of pyrolysis processes performed at temperature higher than 700 °C [28–34], whereas to the best of our knowledge only in one case the pyrolysis temperature was maintained at 600 °C [35]. Conversely, carbonization at mild conditions (i.e., 180–250 °C) were performed only by means of other processes different from pyrolysis (for instance, the hydrothermal carbonization) [29,36,37].

The aim of this work is the preparation and physicochemical characterization of biochars obtained from chitin via pyrolysis at mild conditions (in the 250–550 °C range). Carbonaceous materials were tested as adsorbent substrates for the removal of dyes from aqueous environment. Dyes selected were the cationic methylene blue and the anionic methyl orange. Additionally, adsorption capacities were also evaluated towards the gas phase, measuring the adsorption capacities toward CO_2 and N_2.

Finally, the possibility of using these chars as cathode materials in sustainable and low-cost lithium-sulphur (Li-S) battery system was also reported [38]. Electrochemical reactions in the Li-S battery are multistep reactions with different lithium polysulphides equilibrium states. In the Li-S batteries the main drawback is the polysulphide shuttle phenomena between the cathode and anode with the capacity degradation during cycling. For these reasons, suitable carbon host structures for sulphur with adsorption properties towards lithium polysulphides are constantly under development [39,40] and the synthesis of chitin-derived biochar materials offers real low-cost and easy scalable materials with high N-doped amount for Li-S battery application.

2. Experimental section

2.1. Materials

High purity commercial chitin (from snow crab, CAS 1398-61-4, Heppe Medical Chitosan GmbH) was selected as biochar precursor, whereas commercially available carbon Carboxen 1033 (Spherical carbon molecular sieve, Sigma-Aldrich) was chosen as reference carbon material. Dyes selected for the adsorption testing are: Methylene Blue ($C_{16}H_{18}ClN_3S$, MB in the following, CAS 122965-43-9, purity ≥ 82%, Sigma-Aldrich) and Methyl Orange ($C_{14}H_{14}N_3NaO_3S$, MO in the following, CAS 547-58-0, purity ≥ 85%, Sigma-Aldrich). Other reagents used were: sodium hydroxide (NaOH, purity ≥ 98.0%, CAS 1310-73-2, Sigma-Aldrich), hydrochloric acid (HCl, conc. 37 wt.%, CAS 7647-01-0, Fluka), anhydrous potassium chloride (KCl, CAS 7447-40-7, purity ≥ 99.0%, Fluka), potassium bromide (KBr, FTIR grade ≥ 99%, CAS 7758-02-3, Fluka).

Polyvinylidene fluoride (PVdF, average M_w 534000, CAS 24937-79-9, Sigma-Aldrich) and multi-walled carbon nanotubes (MWCNT, purity ≥ 98.0%, CAS 308068-56-6, Sigma-Aldrich) were used for the electrode preparation. 1 M LiTFSI in TEGME:Diox (purity 99.9%, E057, Solvionic) was used as electrolyte.

All aqueous solutions were prepared using ultrapure water Millipore Milli-Q™. All chemicals were used without further purifications.

2.2. Biochars preparation via pyrolysis

The precursor chitin (ca. 2 g) was thermally treated in a quartz tube reactor LTF 12/38/500 Lenton under nitrogen atmosphere (N_2 flux of 250 mL min^{-1}) with the following thermal program: heating from RT to the target temperature (heating ramp 10 °C min^{-1}), followed by isothermal step for 1 h. Three different target temperatures of pyrolysis were selected: 294 °C (the onset temperature verified experimentally by TGA analysis as the initial temperature of chitin degradation), 440 °C and 540 °C (these two conditions selected at the end of the degradation process). The resulting materials were manually crumbled in an agate mortar for the further characterization and testing. Samples were coded as Ch294, Ch440 and Ch540, depending on the temperature of pyrolysis, whereas the bare chitin was denoted as Ch.

2.3. Physicochemical and morphological characterization

Preliminary thermal analysis was performed by means of a TGA Q600 (TA Instruments) under nitrogen flow (flow rate of 100 mL min^{-1}). The sample mass was kept at about 10 mg in an open alumina pan and heated from RT to 800 °C, heating ramp of 10 °C min^{-1}. Two replicas were performed.

The elemental composition of the solid was determined using a Thermo FlashEA 1112 CHNS–O analyzer. Two replicas were performed and values were presented as% mass mean value ± SD (standard deviation).

Fourier transform infrared (FTIR) spectra were registered in transmission mode using a Bruker Vector 22 spectrophotometer equipped with Globar source, DTGS detector, and working with 128 scans at 4 cm^{-1} resolution in the 4000–400 cm^{-1} range. Chitin and its biochars powders were spectroscopically analyzed as pellets by dispersing the samples in KBr (1:20 wt ratio). Three replicas were performed for each sample.

X-ray diffraction (XRD) patterns were obtained directly on powders by using an PW3040/60 X'Pert PRO MPD diffractometer from PANalytical, equipped with Cu anode, working at 45 kV and 40 mA, in a Bragg-Brentano geometry with a flat sample-holder.

Gas-volumetric analyses were carried out performing N_2 adsorption/desorption experiments at 77 K by means of an ASAP 2020 instrument (Micromeritics) to determine both the specific surface area (BET model) [41] and porosity (DFT model) [42] of the samples. The density functional theory (DFT) was applied in order to consider simultaneously microporosity and mesoporosity. Powdery samples (ca. 0.5–1.0 g) were previously outgassed for about 24 h at 150 °C in vacuum (residual pressure 10^{-2} mbar) to ensure complete removal of atmospheric contaminants from the materials surface before adsorption/desorption experiments [43].

Zeta potential (ζ) measurements were evaluated on the biochars suspensions by means of electrophoretic light scattering (ELS) (Zetasizer Nano–ZS). In this technique, the samples electrophoretic mobility measured by light scattering was proportional to the ζ potential by using the Smoluchowski equation [44]. The ζ potential was measured suspending biochars (ca. 10 mg) in 5 mL of 0.01 M KCl for 24 h, adjusting the pH of suspensions with 0.1 M HCl or 0.1 M NaOH to reach the desired circumneutral condition (pH = 6). This way both the ionic strength and pH were maintained constant during the analysis. Measurements were performed at RT, with an equilibration time of 120 s, and with a cycle of measurement of 5 replicas for each sample. Experiments were run in duplicate and values were presented as charge mean value ± SD (standard deviation).

Scanning electron microscopy (SEM) analyses were carried out by using a ZEISS EVO 50 XVP microscope with LaB_6 source, equipped with detectors for secondary electrons collection and energy dispersive X-ray probe (EDS) for elemental analysis. SEM micrographs were obtained after sputtering samples with ca. 15 nm of a gold layer to avoid any charging effect (Bal-tec SCD050 sputter coater), therefore the presence of gold in EDS spectra (principal signal at 2.2 keV) is due to this step and will not be further investigated.

High-resolution transmission electron microscopy (HRTEM) was used to evaluate the biochars morphology at the nanometric level. Micrographs were obtained by using a JEOL JEM 3010 instrument (300 kV) equipped with a LaB_6 filament coupled with energy-dispersive X-ray probe (EDS). For the specimen preparation, a few drops of biochar-containing water suspensions were poured on holed carbon-coated copper grids and left to RT dry before analyses.

2.4. Isothermal adsorption of dyes from water

Adsorption experiments were performed in separate batch in closed test tubes (containing 10 mL solutions) under continuous shaking at room temperature (RT). Prior to perform the adsorption experiments, ca. 10 mg of biochars were dispersed in 0.01 M KCl solution and the final pH value of 6.0 ± 0.5 was adjusted by drop wise addition of 0.1 M HCl or 0.1 M NaOH solutions (equilibration time was 24 h). In order to optimize the capability of biochars in removing the probe dyes, an initial screening was realized by monitoring the depletion of the dyes main UV–vis signals fixing the dye initial concentration at 100 mg L^{-1}. Additionally, kinetics experiments (not reported for the sake of brevity) were performed by varying the contact time in the 0–24 h range. Experimental evidences confirmed that the adsorption equilibrium was reached at 24 h. The isothermal study was conducted by adding to the suspensions the dye-containing solutions (previously prepared in KCl 0.01 M and at pH = 6) at different concentrations (C_0 from 50 to 1300 mg L^{-1} of dye). Contacts were performed at circumneutral pH, which did not change during the experiments. Afterwards suspensions were shaken in the dark for 24 h at 25 °C. After shaking, 3 mL of supernatants were collected and directly measured by UV–vis spectrophotometry (after performing an external calibration). The absorbance of the two dyes selected for testing were analysed at λ_{max}: namely, 664 nm for MB and 465 nm for MO, using a double-beam spectrophotometer UNICAM UV 300 (Thermospectronic), equipped with both deuterium (for UV) and W (for Vis) lamps, using a PMMA cuvette of 1 cm of optical path.

The amount of dye sorbed (qe, mg g^{-1}) was estimated as follows:

$$qe = [V(C_0\text{-}Ce)]\, m^{-1} \quad (1)$$

C_0 is the initial dye concentration in the solution (mg L^{-1}), Ce is the equilibrium concentration of unadsorbed dye measured by UV–vis analysis (mg L^{-1}), V is the solution volume (10 mL) and m is the sample mass (ca. 10 mg) [45]. To evaluate the efficiency of the sorbing materials, qe can be expressed also in mg m^{-2} by dividing it for the BET specific surface area (m^2 g^{-1}). For the sake of comparison also the performances of a commercial carbon Carboxen 1033 used as adsorbent were studied. Adsorption experiments were performed in duplicate and average values were reported.

To evaluate the regeneration capabilities, desorption experiments were performed for each separate batch by adding the chosen washing medium directly to the wet biochars, submitted to adsorption experiments after filtration, and keeping them in contact under shaking for 24 h at 25 °C in the dark. Two desorption washing media were selected: namely, the first washing step was carried out with 0.01 M KCl at pH = 6, whereas the second one was performed by subsequent washing with 0.1 M NaOH.

2.5. Gas-solid adsorption experiments

Adsorption microcalorimetry was used to measure the heat of adsorption of CO_2 and N_2 at 30 °C. A heat-flow microcalorimeter (Tian-Calvet, Setaram) was employed, following a well-established stepwise procedure, described elsewhere [46,47]. In particular, the calorimeter was connected to a high vacuum volumetric apparatus (residual $p \leq 10^{-5}$ mbar), which enabled to determine simultaneously the adsorbed amounts and the heat evolved at increasing equilibrium pressures for small increments of the adsorptive species. A first adsorption run was performed on ca. 100 mg of sample (primary isotherms), and a second one after pumping off the reversible phase at 30 °C (secondary isotherms), in order to evaluate the irreversible component of the sorption process. The pressure was measured by means of a transducer gauge (Ceramicell, Varian, 0–1000 Torr). For this application, only the sample Ch440 was investigated since this biochar presents the higher specific surface area (*vide infra*), whereas the commercial carbon Carboxen 1033 was used as reference substrate for the sake of comparison.

2.6. Electrochemical characterization of lithium-sulphur batteries

Carbon and sulphur were ball milled in a mass ratio of 40 wt.% of carbon vs. 60 wt.% of sulphur for 30 min at 300 rpm. The carbon/sulphur mixture was transferred into a ceramic crucible and placed into a quartz tube under argon atmosphere. The samples were heated to 155 °C with a heating ramp of 0.2 °C min^{-1}, and held at that temperature for 5 h. The samples were cooled down to RT at 0.5 °C min^{-1}. The electrodes were prepared by mixing the carbon/sulphur composite, the polymer binder polyvinylidene fluoride (PVdF), and the conductive additive multi-walled carbon nanotubes (MWCNT) in a mass ratio of 80:10:10. The slurry was prepared in N-methylpyrolidine (NMP) and casted on carbon coated aluminum foil. The electrodes were dried overnight at 50 °C. The typical sulphur loading on the electrodes were from 1.0 to 1.5 mg per 2 cm^2. The two electrode pouch cells were prepared in an argon filled glovebox. The sulphur cathode (2 cm^2 electrode) was separated from metallic lithium anode with Celgard 2400 wetted with 1 M LiTFSI in TEGDME:Diox (1:1). The electrolyte quantity was normalized to 20 μL per mass of sulphur. The batteries were cycled in the potential range between 1.5 V–3.0 V by using Maccor 4200 galvanostat/potentiostat at a current density of C/10 (167.2 mA g^{-1}).

3. Results and discussion

3.1. Optimization of the pyrolysis process via TGA analysis

TGA analysis of the selected precursor chitin was carried out under nitrogen (inert/reducing) atmosphere in order to simulate the pyrolysis process. Fig. 1 shows the chitin TG profile, which

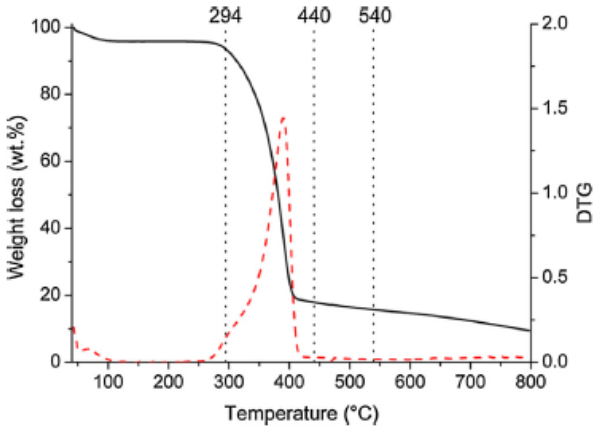

Fig. 1. TG (black solid line) and differential thermal (red dashed line) curves of chitin heated under nitrogen atmosphere. The black dotted lines refer to the three temperatures investigated for the pyrolysis treatments (namely, the onset 294 °C, 440 °C and 540 °C). (For interpretation of the references to colour in this figure legend, the reader is referred to the web version of this article.)

Table 1
Elemental composition of bare chitin (Ch) and its relative biochars (Ch294, Ch440, and Ch540).

Samples	C (wt.%)	H (wt.%)	N (wt.%)	C/N
Ch	43.4	6.4	5.3	8.1
Ch294	47.7	6.3	7.0	6.8
Ch440	72.7	3.5	8.3	8.7
Ch540	75.5	2.8	8.0	9.5

presents two main weight losses: the first one due to the water evaporation (centered at ca. 100 °C), and the second one mainly due to the degradation phenomena of the polysaccharide structure (in the 290–400 °C range). Basing on the DTG profile, it is possible to evaluate both the onset temperature (i.e., the initial temperature of material degradation) and the maximum rate of decomposition temperature (which corresponds to the maximum of the DTG curve), which are 294 °C and 390 °C, respectively. A carbonaceous residue, which represented ca. the 4.6 ± 0.6 wt.% of the starting sample, was collected at 800 °C. According to the literature [17], the degradation mechanism of chitin favored the formation of H_2O, CO_2, CO, and CH_3COOH, whereas ammonia does not seem to be released since the fate of the nitrogen is preferentially the formation of N-containing heterocyclic rings (such as pyrazine, pyridine, and pyrrole moieties) included in the carbonaceous residue and/or subsequently released as volatiles. These results encourage the use of chitin as green sustainable precursor for the production of N-doped carbons. Thus, in order to convert chitin into biochar without excessive nitrogen-loss and also trying to maintain the largest amount of residual functionalities, pyrolysis of chitin was performed at mild conditions. In detail, three different pyrolysis temperatures were investigated: the onset temperature (294 °C), and two temperatures after the main degradation phenomenon, namely 440 °C and 540 °C.

3.2. Physicochemical and morphological characterization of biochars

The elemental analysis of chitin and its biochars is reported in Table 1. In general, with respect to the initial precursor, it is possible to observe that the elemental composition of the sample produced at the onset temperature Ch294 (47.7 wt.% of C, 6.3 wt.% of H, and 7.0 wt.% of N) is almost similar to that of the neat chitin (43.4 wt.% of C, 6.4 wt.% of H, and 5.3 wt.% of N), suggesting the high thermal stability of the starting biopolymer.

Biochars produced at higher pyrolysis temperatures (i.e., 440 °C and 540 °C) show a significant increase of the C amount with the pyrolysis temperature (72.7 wt.% and 75.5 wt.%, respectively), whereas the nitrogen content is in the 7.0–8.3 wt.% range. Other samples described in the literature [29] present a better efficiency in the carbonization process showing a higher amount of carbon, but a direct and significant comparison is not possible because the pyrolysis conditions applied were very different.

In order to unveil the pyrolysis-induced chemical modifications and the chitin-to-biochar conversion mechanism induced by the different pyrolysis conditions, both FTIR spectroscopy (Fig. 2A) and XRD analyses (Fig. 2B) were performed on the three samples (Ch294, Ch440, and Ch540), and data compared to those of the neat precursor (Ch).

The FTIR spectrum of chitin before pyrolysis (Ch) displays the narrow peaks assigned to the crystalline polysaccharide structure. The main signals in the spectrum are: a strong and broad band at ca. 3440 cm^{-1} associated to the axial O—H and N—H stretching modes, followed by a signal at 2880 cm^{-1} due to C—H stretching mode (Fig. 2A, green box), the absorption bands at 1660 and 1630 cm^{-1} attributable to the axial C═O stretching of the acetamido moieties (amide I), together with the one at 1580 cm^{-1} due to the angular deformation of N—H bonds of the amino groups (amide II) (Fig. 2A, red box), the bands in the 1450–1350 cm^{-1} range assigned to the —CH_3 symmetrical deformation mode, and the finger print bands at 1150–900 cm^{-1} range due to C—O and C—O—C stretching mode of the glycosidic ring (Fig. 2**A**, blue box) [48]. In particular, according to the literature the two crystalline phases (α-chitin and β-chitin) can be recognized by means of the FTIR analysis looking at the amide I and II bands. In fact, in α-chitin the amide I band is splitted into two signals at 1660 and 1630 cm^{-1} [49], whereas the amide II band is centered at 1558 cm^{-1}. Conversely, β-chitin presents only one signal due to amide I at 1630 cm^{-1}, whereas the amide II band is shifted to 1562 cm^{-1} [48]. Hence, on the basis of amide I and II infrared vibrations here detected, it is possible to assume that the precursor selected in this study is made by α-chitin. Additionally, amide I and II bands are also important for the determination of the DD. Although, in our previous study we already determined the chitin DD by means of TGA-FTIR (after previous calibration with ^1H NMR) being 54% [17].

The sample Ch294 obtained after pyrolysis at the onset temperature (294 °C) still maintains the main signals due to chitin functionalities, and this is in agreement with the elemental analysis. Conversely, the two samples obtained at higher pyrolysis temperatures (440–540 °C) evidence the loss of all the main relevant bands associated to chitin functional groups, with the formation of a single broad signal in the 1600–1000 cm^{-1} range associated to the formation of C—C and C═C bonds of a carbonaceous structure (Fig. 2A, violet box) [50]. Moreover, no further substantial structural and chemical modifications were registered between the two FTIR spectra of samples Ch440 and Ch540 (and this is consistent with the TGA analysis in Fig. 1), apart from a slight reduction of the relative intensity of the bands at ca. 3440 cm^{-1} due to —OH and —NH stretching modes by increasing the pyrolysis temperature, confirming a further loss of heteroatoms (as already evidenced by the elemental analysis).

The XRD pattern of bare chitin is reported in Fig. 2B. All the crystalline planes reflection registered for such sample at 2θ = 9.3° (020), 12.7° (101), 19.2° (040) and (110), 23.2° (130), and 26.3° (013) are consistent with the presence of the α-phase of chitin (card number 00-035-1974 from the ICCD Database) [51]. The α-phase evidenced by XRD is also consistent with the position of amide I and II bands in the FTIR spectrum. Nevertheless, in analogy with both elemental analysis and FTIR spectroscopy, the sample obtained at

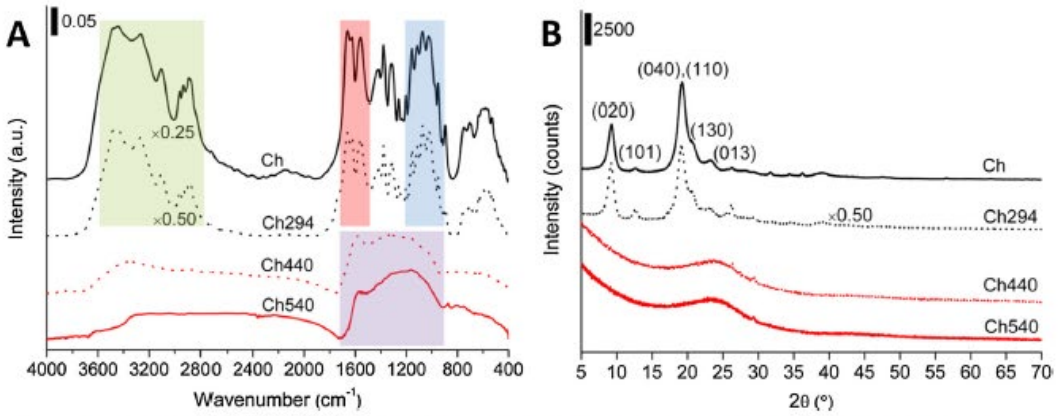

Fig. 2. Physicochemical characterization of bare chitin and its relative biochars (Ch294, Ch440, and Ch540). Panel A: Absorbance FTIR spectra in the 4000–400 cm^{-1} range relative to chitin (Ch, black solid line), Ch294 (black dotted line), Ch440 (red dotted line), and Ch540 (red solid line). The main relevant peaks are labeled. All spectra are collected in transmission mode through KBr pellets. Panel B: XRD patterns of the chitin (Ch, black solid line), Ch294 (black dotted line), Ch440 (red dotted line), and Ch540 (red solid line). The main reflections due to chitin crystalline structure are highlighted and labeled. (For interpretation of the references to colour in this figure legend, the reader is referred to the web version of this article.)

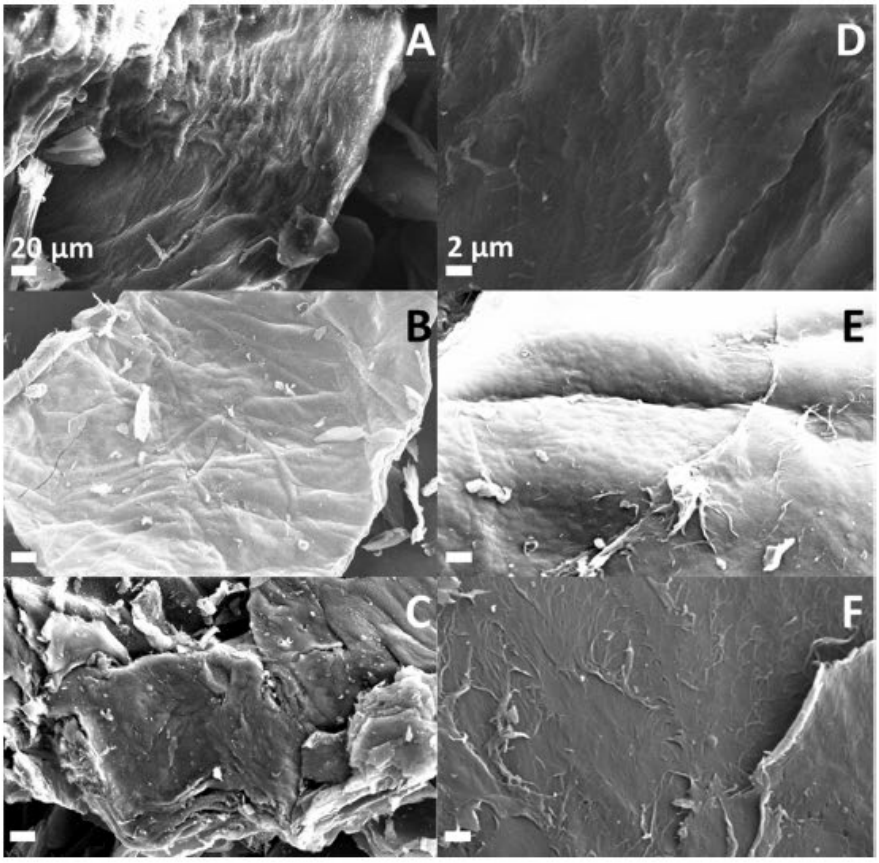

Fig. 3. SEM micrographs at low (left) and high (right) magnification of Ch294 (A,D), Ch440 (B,E), and Ch540 (C,F).

the onset temperature Ch294 presents the same XRD pattern as bare chitin, suggesting the absence of any structural modifications. Samples obtained after pyrolysis at 440 °C and 540 °C evidenced the complete loss of the crystalline reflections due to chitin ordered structure and the formation of a broad amorphous signal centered at 2θ – 23–25°. Additionally, two weak shoulders were registered at ca. 2θ – 26° and 29°, which can be assigned respectively to the formation of the (002) graphitic basal plans in the biochars [52] and to residual inorganic $CaCO_3$ from the demineralization process of crab shells [53,54].

In order to evaluate the morphology of materials, SEM analyses were performed on all chitin-derived biochars. In all cases, the materials surface shows at low magnification (Fig. 3A–C) a certain degree of roughness, with the presence of few defects and cracks.

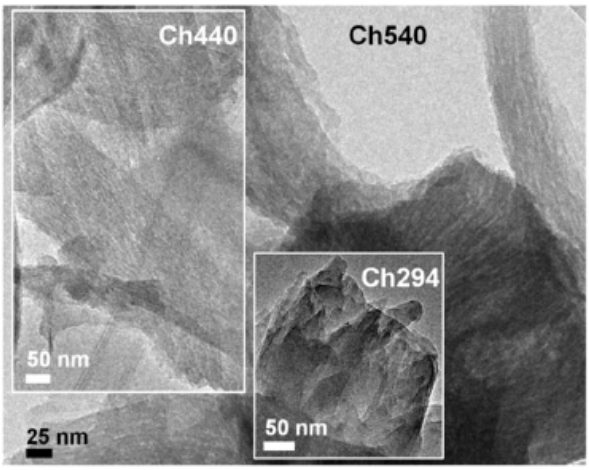

Fig. 4. HRTEM micrographs of Ch294, Ch440, and Ch540.

Samples obtained after pyrolysis at higher temperatures show the formation of some filaments crossing the surface at high magnification (Fig. 3D–F).

HRTEM images of all samples are reported in Fig. 4. Ch294 is made of large, disordered, dense, almost aggregated patches, whereas both samples prepared by pyrolysis at high temperatures (i.e., Ch440, and Ch540) evidenced the formation of amorphous elongated particles, and some structural order can be perceived in some parts of the materials, in agreement with the XRD profiles. This trend suggests the beginning of the graphitization process (in accordance to XRD peak at $2\theta = 26^{\circ}$), which is usually expected at higher temperatures ($T = 750–1000\,^{\circ}C$) [4].

Nitrogen sorption measurements at 77 K were performed on all chitin-derived biochars and reference Carboxen 1033, and results (in terms of specific surface area and pore volume) are summarized in Table 2. Considering the simultaneous presence of micro and mesoporosities (as evidenced by the pore size distribution curves) in all samples, Langmuir model was excluded for calculation of specific surface area and BET data are reported in Table 2. Only the two samples obtained at high pyrolysis temperatures (Ch440 and Ch540) present relevant values of BET specific surface area and porosity. According to the IUPAC classification, both isotherms (not reported for the sake of brevity) show a profile IV, with a hysteresis loop of type H4 frequently associated to slit-shaped mesopores. Additionally, the presence of a pronounced knee in the initial part of the isotherms suggested the presence of a certain degree of microporosity. The pore size distribution (Table 2) indicated the presence of two families of micropores and small mesopores. In order to evaluate the surface charge of the biochars produced, measurements of zeta potential were performed maintaining constant the ionic strength (0.01 M KCl) and the pH (pH = 6). Values of zeta potential measured for all biochars (Ch294, Ch440, and Ch540) and the reference Carboxen 1033 were reported in Table 2. At the first sight, all carbonaceous materials are characterized by a negatively charged surface, following the order Ch440 ≥ Carboxen 1033 > Ch294 > Ch540 in terms of absolute values. The zeta potential variation with the increasing of the pyrolysis temperature can be explained considering the chemical modifications induced by the thermal treatments, i.e., loss of the functional groups.

3.3. Aqueous dyes adsorption-desorption experiments

Adsorption experiments were performed in order to evaluate the potential application of chitin-derived biochars for the removal of pollutants from contaminated water at circumneutral pH. Adsorption-desorption experiments were performed on two model dyes: MB, cationic, and MO, anionic. The spectroscopic calibration curves of both dyes were reported in Fig. S**1** (λ_{max}(MB) = 664 nm) and Fig. S**2** (λ_{max}(MO) = 465 nm).

Adsorption experiments were performed in isothermal conditions in separate batch in closed test tubes (containing 10 mL solutions) under continuous stirring at 25 °C. Kinetics experiments were performed by varying the contact time in the 0–24 h range (see for instance the MB-Ch440 performances in Fig. S**3**). Experimental evidences confirmed that the adsorption equilibrium was reached at 24 h. Thus, by fixing both the sorbent concentration (1000 mg L^{-1}) and the optimized contact time (24 h), equilibrium isotherms were carried out at different dyes concentration (C_0 = 50–1300 mg L^{-1}), maintaining constant the temperature (25 °C, in the dark), the ionic strength (i.e., [KCl] = 0.01 M), and the pH (pH = 6).

Prior to isothermal studies, a preliminary screening was realized fixing the initial dye concentration (C_0 = 100 mg L^{-1}). Results evidenced that all three biochars are good adsorbents respect to both dyes (Fig. 5A and C), and that the best performances were reached for both Ch440 and Ch540.

The adsorption isothermal curve profiles (expressed as mg g^{-1} vs. mg L^{-1}) are reported in Fig. 5B (MB) and D (MO). Results evidenced that the best adsorption performances among the chitin-derived biochars were reached by Ch440 for MB (qe = 26.7 mg g^{-1}) and by Ch540 for MO (qe = 16.0 mg g^{-1}). These results can be explained considering two factors.

i) On one hand the electrostatic component is one of the main driving forces of the adsorption process. In fact, the best sorption performances against the cationic dye MB were reached by the more negatively charged biochar Ch440 (−31.0 mV), whereas the negatively charged dye MO surely experiments a certain repulsive component in the sorption mechanism toward the negatively charged surface of all biochars: in this situation the best performances were reached by the sample with the less negatively charged surface Ch540 (−18.5 mV).

ii) On the second hand, it is necessary to consider the different specific surface areas of the three samples, and this explains the best performances obtained for Ch440 and Ch540.

Interestingly, expressing the adsorbed amount qe as mg m^{-2} (see Fig. S**4**), it is possible to evidence that the sample with the lowest surface area Ch294 has the highest affinity for both dyes (qe = 2.5 mg m^{-2} for MB and 1.0 mg m^{-2} for MO), even more pronounced than that observed for the reference Carboxen 1033 (qe = 0.2 mg m^{-2} for MB and ca. 0.1 mg m^{-2} for MO). This indicates that the lowest the pyrolysis condition, the better the affinity of the material surface towards the polar chemical substrates, as expected due to the presence of residual polar functional groups on Ch294. This result suggests to continue the optimization of the pyrolysis conditions in order to reach the best compromise between a high polarity of the surface (i.e., low pyrolysis temperature) and a high surface development (obtained at higher pyrolysis temperature).

Desorption experiments were performed on Ch440, chosen as reference substrate. As reported in the Experimental section, desorption trials were carried out in two following steps: by washing the wet material with a solution of 0.01 M KCl (at pH = 6) and, subsequently, with a solution of 0.1 M NaOH. The results obtained are summarized in Fig. 6 and clearly evidences that the cationic dye MB is almost irreversibly bonded to the negatively charged surface of Ch440, since no removal of the adsorbed dye is observed for KCl washing and only an amount <10% is removed in the presence of NaOH. Otherwise, as expected, the anionic dye MO, which is weakly sorbed at the biochar negative surface, shows a regeneration procedure more effective (about 20% is removed after KCl washing and up to 60% is removed in the presence of NaOH).

Table 2
BET surface area, DFT pore volume (micro, meso and total), and zeta potential measured for the chitin-derived biochars (Ch294, Ch440, and Ch540) and the reference commercial material Carboxen 1033.

Samples	BET surface area ($m^2\,g^{-1}$)	DFT pore volume ($cm^3\,g^{-1}$)		Zeta potential ζ (mV ± SD)[c]
		Micropores	Mesopores	
Carboxen 1033	420[a]	0.15	0.10	−26.2 ± 1.7
Ch294	8[b]	–	–	−19.0 ± 1.3
Ch440	338	0.08	0.11	−31.0 ± 1.7
Ch540	333	0.09	0.08	−18.5 ± 1.0

[a] Carboxen 1033 characteristics are taken directly from the Sigma-Aldrich database.
[b] The BET specific surface area of Ch294 is below the instrumental limit therefore the value reported is only approximative.
[c] The ζ potential was measured maintaining constant the biochar concentration, ionic strength (0.01 M KCl), and pH (pH = 6). Experiments were run in duplicate and values were presented as mean value ± SD (standard deviation).

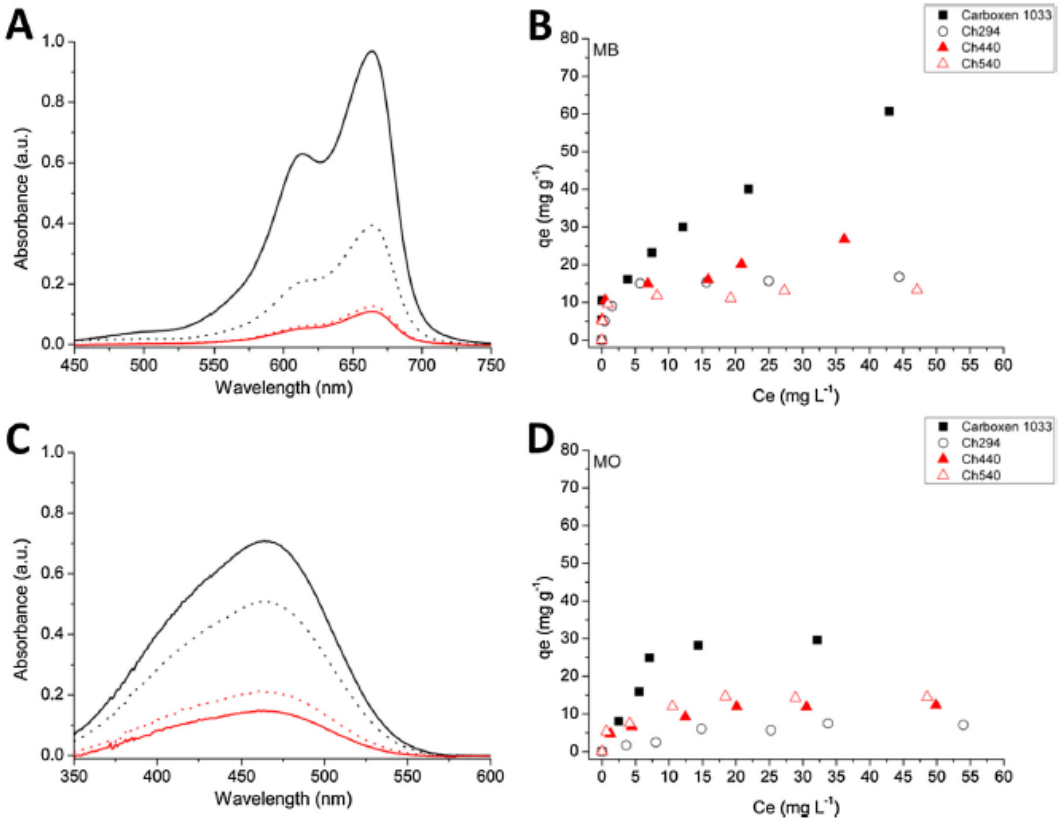

Fig. 5. UV–vis spectra of the aqueous solution (left), and adsorption isotherms (right) of MB (top) and MO (bottom) on chitin-derived biochars (expressed as mg g^{-1} vs. mg L^{-1}). Panels A, C: Initial screening. Legend: Blank test without biochar (black solid curve), Ch294 (black dotted line), Ch440 (red dotted line), and Ch540 (red solid line). Experimental conditions: [sorbent] = 1000 mg L^{-1}, [dye] = 100 mg L^{-1}, contact time = 24 h, [KCl] = 0.01 M, T = 25 °C, pH = 6. Panels B, D: Adsorption isotherms. Legend: Carboxen 1033 (black squares), Ch294 (white circles), Ch440 (red triangles), and Ch540 (white triangles). Experimental conditions: [sorbent] = 1000 mg L^{-1}, [dye] = 50–1300 mg L^{-1}, contact time = 24 h, [KCl] = 0.01 M, T = 25 °C, pH = 6. (For interpretation of the references to colour in this figure legend, the reader is referred to the web version of this article.)

These tests, although preliminary, confirmed that such chitin-derived biochars obtained at mild conditions (in particular those obtained from pyrolysis at 440–540 °C) are sorbing materials promising for the removal of charged species from contaminated water, which are immobilized at the carbon surface if positively charged, whereas it is possible to evidence an interesting recycling capacity of the materials in the presence of negatively charged contaminants.

3.4. Microcalorimetry performances of chitin-derived biochar

In order to evaluate the capacity of such biochars as sequestrating agents of CO_2 molecules from the gas phase, microcalorimetric experiments were performed on the chitin-derived material with the highest BET surface area value, namely Ch440 (338 $m^2\,g^{-1}$). Fig. 7A reports the gas-volumetric isotherms obtained at 30 °C in the p_{CO2} range 0–500 Torr. The comparison between primary and secondary runs evidences that the adsorption is completely reversible suggesting an easy regeneration of the material. Sorption curves show the typical hyperbolic trend and their shape suggests an high sorption capacity, since they are still far from the saturation level. Fig. 7B reports the molar heat of adsorption measured for the sample as a function of coverage. The values are almost constant in the 50–60 kJ mol^{-1} range, indicating a high energetic homogeneity of the surface and confirming the possibility of regenerating the material after CO_2 storage given the not too high interaction energy

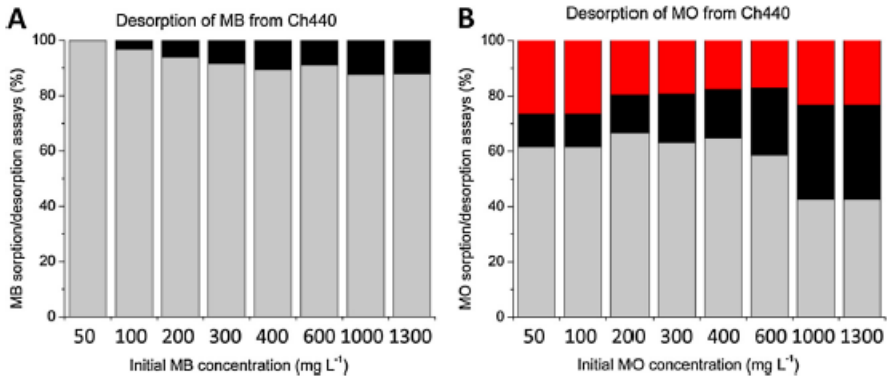

Fig. 6. Desorption experiments of MB (A, left) and MO (B, right) from Ch440. Legend: residual dye irreversibly bonded to the sorbent surface (grey), dye removed after washing with 0.01 M KCl at pH = 6 (black) and after subsequent washing with 0.1 M NaOH (red). Experimental conditions: [sorbent] = 1000 mg L^{-1}, contact time = 24 h, T = 25 °C. (For interpretation of the references to colour in this figure legend, the reader is referred to the web version of this article.)

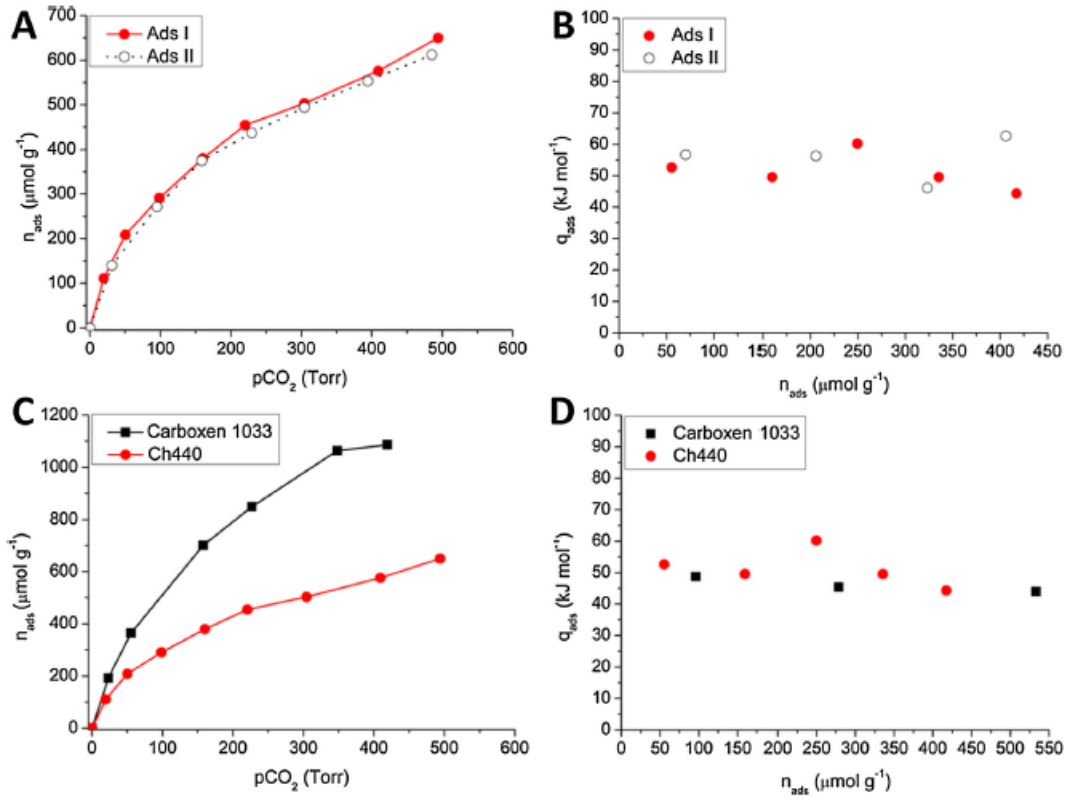

Fig. 7. Microcalorimetric analysis. Gas-volumetric isotherms expressed as adsorbed amounts n_{ads} vs. equilibrium pressure of CO_2 (A) and molar heat of adsorption as a function of CO_2 uptake (B) on Ch440 outgassed at T = 303 K. Legend: Ads I (red circles, red solid line), and Ads II (white circles, black dotted line). Comparison in terms of volumetric isotherms (C) and heat of adsorption (D) between Carboxen 1033 and Ch440 outgassed at T = 303 K (Ads I). Legend: Carboxen 1033 (black squares, black solid line), and Ch440 (red circles, red solid line). (For interpretation of the references to colour in this figure legend, the reader is referred to the web version of this article.)

observed. For the sake of comparison, the performance of Ch440 was compared with that of the reference commercial carbon Carboxen 1033. The obtained results indicate that the sorption capacity of Ch440 is promising if compared to the reference Carboxen 1033. In fact, even though Carboxen 1033 presents higher adsorption capacity (almost twice the Ch440 one, as evidenced in Fig. 7C), the energetic feature is similar (Fig. 7D). Finally, to evaluate the selectivity of Ch440 towards CO_2 adsorption, a microcalorimetric measurement was performed using N_2 as gas probe. The adsorbed amounts and adsorption heats gave negligible values (not reported for the sake of brevity), as in the case of Carboxen 1033. These results indicate that Ch440 can reversibly and selectively interact with CO_2, being potentially useable for environmental applications as sequestering agent for reducing the emission of greenhouse gases (such as CO_2).

3.5. *Electrochemical characterization of Li-S battery*

The chitin-derived biochars (Ch294, Ch440 and Ch540) were impregnated with 60 wt.% of sulphur (denoted as S/sample name)

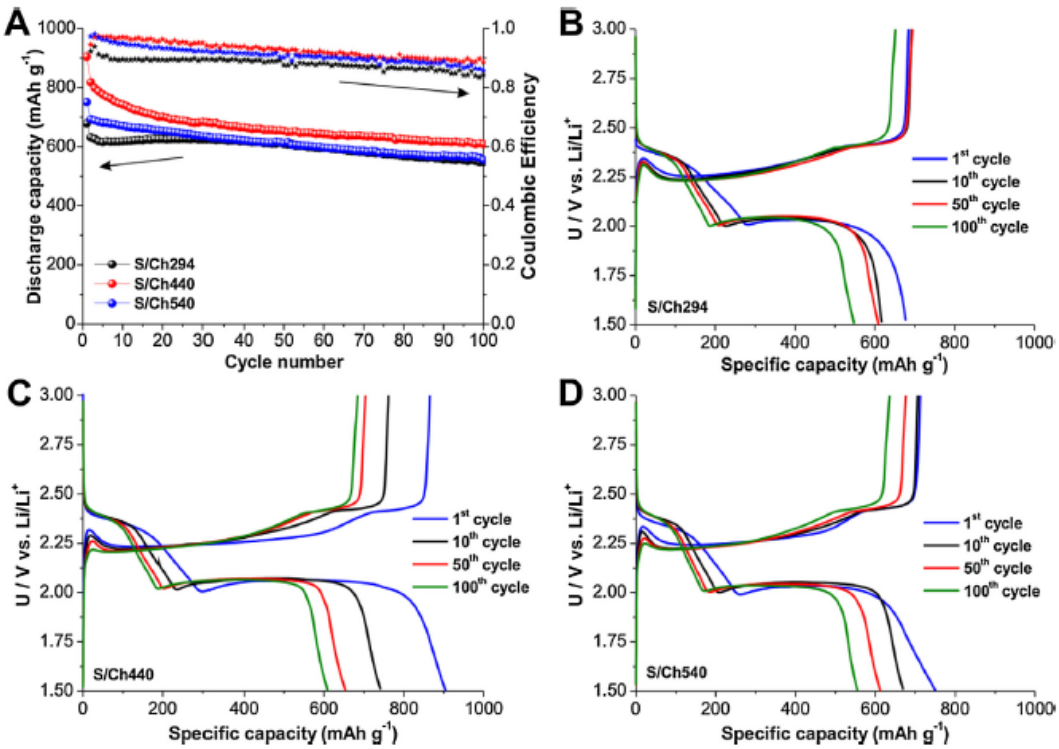

Fig. 8. Li-S battery with chitin-derived biochar carbon host material; (A) discharge cycling properties (left axis) and coulombic efficiency (right axis) at current density C/10 and galvanostatic curves for the 1st, 10th, 50th and 100th cycle for (B) Ch294, (C) Ch440, (D) Ch540.

and tested as cathode material in Li-S batteries (Fig. 8). The Fig. 8A shows the obtained discharge capacities and coulombic efficiency for the three sulphur/chitin-derived biochar composites. The highest initial discharge capacity reaching 905 mAh g^{-1} was obtained with S/Ch440. However, the S/Ch440 shows an initial rapid loss in capacity in the initial cycles. After 50th and 100th cycles, a retained capacity of 654 mAh g^{-1} and 610 mAh g^{-1} with a coulombic efficiency around 90% was obtained. The S/Ch540 shows lower initial discharge capacity of 751 mAh g^{-1} and a retained capacity of 612 mAh g^{-1} after 50th cycles and 555 mAh g^{-1} after 100th cycles with a coulombic efficiency around 89%. The S/Ch294 has the lowest initial discharge capacity of 679 mAh g^{-1}. On the other hand, the S/Ch294 shows a stable cycling behavior in the initial cycles with a retained capacity of 609 mAh g^{-1} after 50th cycles and 548 mAh g^{-1} after 100th cycles with a coulombic efficiency around 86%. The initial stable capacity of the S/Ch294 is due to the remaining oxygen and nitrogen functional groups, which have chemisorption affinity towards the lithium polysulphides [55].

Fig. 8B–C shows the galvanostatic curves for the sulphur/chitin-derived biochar composites. The voltage profiles of the batteries have a characteristic Li-S signature. In the high-voltage plateau at around 2.4 V the long-chain lithium polysulphides are formed out of the elemental sulphur. In the transition state from 2.4 V to 2.1 V, the long-chain lithium polysulphides are reduced into the shorter lithium polysulphides. In the low-voltage plateau at around 2.1 V the short-chain lithium polysulphides are in the equilibrium state with the lithium sulphide (Li_2S) precipitation [56,57]. Further analyses of the discharge and charge curves in Fig. 8B–C show that the polarization is not increased during cycling. The sample produced at the onset temperature Ch294 exhibits in the Li-S battery the highest polarization value of 142 mV. This is due to the lower temperature of pyrolysis. The Ch440 and Ch540 show lower polarization and higher coulombic efficiency, which is attributed to improved electron transfer, due to higher pyrolysis temperature and higher conductivity. Moreover, the higher amount of nitrogen doping in the chitin-derived biochars increases the adsorption towards the lithium polysulphides that results in better capacity retention during cycling [39].

4. Conclusions

In this work, chitin (a biopolymer obtained from shellfish industry) was used as precursor for the production of biochars obtained via pyrolysis treatment performed at mild conditions. Basing on TGA analyses carried out under nitrogen (inert/reducing) atmosphere, temperatures selected for the pyrolysis processes are the chitin decomposition onset temperature (294 °C), and two temperatures after the main degradation phenomenon, namely 440 °C and 540 °C. All biochars prepared were physicochemical characterized, in order to evaluate the pyrolysis-induced effects in terms of both functional groups and materials structure.

Moreover, carbonaceous materials were tested as adsorbent substrates for the removal of target molecules (cationic MB and anionic MO dyes) from aqueous environment. Experiments evidenced good adsorption capacities, modulable regeneration features and some hints for driving the optimization of the materials towards molecules adsorption. Additionally, adsorption capacities were also evaluated towards gaseous CO_2 with promising results. Finally, biochars were investigated as possible cathode materials in sustainable and low-cost lithium-sulphur (Li-S) batteries. Experimental results evidenced that biochar produced at the onset temperature Ch294 exhibits high polarization and initial stable discharge capacity, whereas Ch440 and Ch540 show lower polarization with higher and stable discharge capacities and higher coulombic efficiencies during prolong cycling.

Therefore, in this study chitin-derived biochars offer sustainable, low-cost and easy scalable alternative carbonaceous materials, which can be used in environmental remediation treatments (both in liquid and gaseous phases), as well as for electrochemical energy storage devices in Li-S batteries.

Acknowledgements

This work was realized with the financial support for academic interchange by the Marie Sklodowska-Curie Research and Innovation Staff Exchange project funded by the European CommissionH2020-MSCA-RISE-2014 within the framework of the research project Mat4treaT (Project number: 645551). Compagnia di San Paolo and University of Torino are gratefully acknowledged for funding Project Torino_call2014_L2_126 through "Bando per il finanziamento di progetti di ricerca di Ateneo – anno 2014" (Project acronym: Microbusters). Additionally, authors would like to acknowledge Prof. Domenica Scarano, Dr. Federico Cesano, Dr. Enzo Laurenti and Mr. Riccardo Leinardi (University of Torino, Italy) for practical support in the use of helpful instruments. AV thanks Tjaš Cvek for the help in the laboratory, Prof. Dr. Robert Dominko for useful discussions and the European Union Horizon 2020 framework under grant agreement no. 666221 (HELIS) for founding.

Appendix A. Supplementary data

Supplementary data associated with this article can be found, in the online version, at http://dx.doi.org/10.1016/j.apsusc.2017.07.277.

References

[1] J. Lehmann, S. Joseph, Biochar for environmental management: an introduction, in: J. Lehmann, S. Joseph (Eds.), Biochar for Environmental Management Science and Technology, Earthscans, UK, 2009, pp. 1–12.
[2] IBI, Standardized Product Definition and Product Testing Guidelines for Biochar That Is Used in Soil, International Biochar Initiative, 2012 (April 2012).
[3] E. Fitzer, K.-H. Köchling, H.P. Boehm, H. Marsh, Recommended terminology for the description of carbon as a solid (IUPAC Recommendations 1995), Pure Appl. Chem. 67 (1995) 473–506.
[4] M.-M. Titirici, R.J. White, N. Brun, V.L. Budarin, D. Sheng Su, F. del Monte, J.H. Clark, M.J. MacLachlan, Sustainable carbon materials, Chem. Soc. Rev. 44 (2015) 250–290.
[5] P. Xiong, Y. Fu, L. Wang, X. Wang, Multi-walled carbon nanotubes supported nickel ferrite: A magnetically recyclable photocatalyst with high photocatalytic activity on degradation of phenols, Chem. Eng. J. 195–196 (2012) 149–157.
[6] Z. Wang, L. Qie, L. Yuan, W. Zhang, X. Hu, Y. Huang, Functionalized N-doped interconnected carbon nanofibers as an anode material for sodium-ion storage with excellent performance, Carbon 55 (2013) 328–334.
[7] Y. Fu, J. Zhu, C. Hu, X. Wu, X. Wang, Covalently coupled hybrid of graphitic carbon nitride with reduced graphene oxide as a superior performance lithium-ion battery anode, Nanoscale 6 (2014) 12555–12564.
[8] R.J. White, V. Budarin, R. Luque, J.H. Clark, D.J. Macquarrie, Tuneable porous carbonaceous materials from renewable resources, Chem. Soc. Rev. 38 (2009) 3401–3418.
[9] R. Kumar, R. Kumar Singh, D. Pratap Singh, Natural and waste hydrocarbon precursors for the synthesis of carbon based nanomaterials: graphene and CNTs, Renew. Sustain. Energy Rev. 58 (2016) 976–1006.
[10] M. Sevilla, A.B. Fuertes, Chemical and structural properties of carbonaceous products obtained by hydrothermal carbonization of saccharides, Chemistry-A Eur. J. 15 (2009) 4195–4203.
[11] K. Anastasakis, A.B. Ross, J.M. Jones, Pyrolysis behaviour of the main carbohydrates of brown macro-algae, Fuel 90 (2011) 598–607.
[12] J. Deng, M. Li, Y. Wang, Biomass-derived carbon: synthesis and applications in energy storage and conversion, Green Chem. 18 (2016) 4824–4854.
[13] M. Zanetti, A. Anceschi, G. Magnacca, G. Spezzati, F. Caldera, G.P. Rosi, F. Trotta, Micro porous carbon spheres from cyclodextrin nanosponges, Microporous Mesoporous Mater. 235 (2016) 178–184.
[14] S. Hajji, I. Younes, O. Ghorbel-Bellaaj, R. Hajji, M. Rinaudo, M. Nasri, K. Jellouli, Structural differences between chitin and chitosan extracted from three different marine sources, Int. J. Biol. Macromol. 65 (2014) 298–306.
[15] F.A. Al Sagheer, M.A. Al-Sughayer, S. Muslim, M.Z. Elsabee, Extraction and characterization of chitin and chitosan from marine sources in Arabian Gulf, Carbohydr. Polym. 77 (2009) 410–419.
[16] F.M. Kerton, Y. Liu, K.W. Omari, K. Hawboldt, Green chemistry and the ocean-based biorefinery, Green Chem. 15 (2013) 860–871.
[17] I. Corazzari, R. Nisticò, F. Turci, M.G. Faga, F. Franzoso, S. Tabasso, G. Magnacca, Advanced physico-chemical characterization of chitosan by means of TGA coupled on-line with FTIR and GCMS: thermal degradation and water adsorption capacity, Polym. Degrad. Stab. 112 (2015) 1–9.
[18] R.A.A. Muzzarelli, Chitin, Pergamon Press Ltd, U.K. Oxford, 1977.
[19] M. Rinaudo, Chitin and chitosan: properties and applications, Prog. Polym. Sci. 31 (2006) 603–632.
[20] S. Babel, T.A. Kurniawan, Low-cost adsorbents for heavy metals uptake from contaminated water: a review, J. Hazard. Mater. 97 (2003) 219–243.
[21] W.S. Wan Ngah, L.C. Teong, M.A.K.M. Hanafiah, Adsorption of dyes and heavymetal ions by chitosan composites: a review, Carbohydr. Polym. 83 (2011) 1446–1456.
[22] S. Ladet, L. David, A. Domard, Multi-membrane hydrogel, Nature 452 (2008) 76–79.
[23] P. Avetta, R. Nisticò, M.G. Faga, D. D'Angelo, E. Aimo Boot, R. Lamberti, S. Martorana, P. Calza, D. Fabbri, G. Magnacca, Hernia-repair prosthetic devices functionalised with chitosan and ciprofloxacin coating: controlled release and antibacterial activity, J. Mater. Chem. B 2 (2014) 5287–5294.
[24] R. Nisticò, M.G. Faga, G. Gautier, G. Magnacca, D. D'Angelo, E. Ciancio, G. Piacenza, R. Lamberti, S. Martorana, Physico-chemical characterization of functionalized polypropylenic fibers for prosthetic applications, Appl. Surf. Sci. 258 (2012) 7889–7896.
[25] E.I. Rabea, M.E.T. Badawy, C.V. Stevens, G. Smagghe, W. Steurbaut, Chitosan as antimicrobial agent: applications and mode of action, Biomacromolecules 4 (2003) 1457–1465.
[26] F. Cesano, G. Fenoglio, L. Carlos, R. Nisticò, One-step synthesis of magnetic chitosan polymer composite films, Appl. Surf. Sci. 345 (2015) 175–181.
[27] R. Nisticò, F. Franzoso, F. Cesano, D. Scarano, G. Magnacca, L. Carlos, M.E. Parolo, Chitosan-derived iron oxide systems for magnetically-guided and efficient water purification processes from polycyclic aromatic hydrocarbons, ACS Sustainable Chem. Eng. 5 (2017) 793–801.
[28] T.-D. Nguyen, K.E. Shopsowitz, M.J. MacLachlan, Mesoporous nitrogen-doped carbon from nanocrystalline chitin assemblies, J. Mater. Chem. A 2 (2014) 5915–5921.
[29] H. Yuan, L. Deng, X. Cai, S. Zhou, Y. Chen, Y. Yuan, Nitrogen-doped carbon sheets derived from chitin as non-metal bifunctional electrocatalysts for oxygen reduction and evolution, RSC Adv. 5 (2015) 56121–56129.
[30] B. Duan, X. Gao, X. Yao, Y. Fang, L. Huang, J. Zhou, L. Zhang, Unique elastic N-doped carbon nanofibrous microspheres with hierarchical porosity derived from renewable chitin for high rate supercapacitors, Nano Energy 27 (2016) 482–491.
[31] Y. Gao, S. Xu, Q. Yue, Y. Wu, B. Gao, Chemical preparation of crab shell-based activated carbon with superior adsorption performance for dye removal from wastewater, J. Taiwan Inst. Chem. Eng. 61 (2016) 327–335.
[32] J. Qu, S. Lv, X. Peng, S. Tian, J. Wang, F. Gao, Nitrogen-doped porous green carbon derived from shrimp shell: combined effects of pore sizes and nitrogen doping on the performance of lithium sulfur battery, J. Alloys Compd. 671 (2016) 17–23.
[33] L. Wang, Y. Zheng, X. Wang, S. Chen, F. Xu, L. Zuo, J. Wu, L. Sun, Z. Li, H. Hou, Y. Song, Nitrogen-doped porous carbon/Co_3O_4 nanocomposites as anode materials for lithium-ion batteries, ACS Appl. Mater Interfaces 6 (2014) 7117–7125.
[34] J. Qu, C. Geng, S. Lv, G. Shao, S. Ma, M. Wu, Nitrogen, oxygen and phosphorus decorated porous carbons derived from shrimp shells for supercapacitors, Electrochim. Acta 176 (2015) 982–988.
[35] M. Nogi, F. Kurosaki, H. Yano, M. Takano, Preparation of nanofibrillar carbon from chitin nanofibers, Carbohydr. Polym. 81 (2010) 919–924.
[36] R.J. White, M. Antonietti, M.-M. Titirici, Naturally inspired nitrogen doped porous carbon, J. Mater. Chem. 19 (2009) 8645–8650.
[37] G. Gedda, C.-Y. Lee, Y.-C. Lin, H.-F. Wu, Green synthesis of carbon dots from prawn shells for highly selective and sensitive detection of copper ions, Sens. Actuators B 224 (2016) 396–403.
[38] S. Evers, L.F. Nazar, New approaches for high energy density lithium–sulfur battery cathodes, Acc. Chem. Res. 46 (2013) 1135–1143.
[39] F. Schipper, A. Vizintin, J. Ren, R. Dominko, T.-P. Fellinger, Biomass-derived heteroatom-doped carbon aerogels from a salt melt sol–gel synthesis and their performance in Li–S batteries, ChemSusChem 8 (2015) 3077–3083.
[40] A. Roseman, E. Markevich, G. Salitra, D. Aurbach, A. Garsuch, F.F. Chesneau, Review on Li-Sulfur battery systems: an integral perspective, Adv. Energy Mater. 5 (2015), http://dx.doi.org/10.1002/aenm.201500212.
[41] S. Brunauer, P.H. Emmett, E. Teller, Adsorption of gases in multimolecular layers, J. Am. Chem. Soc. 60 (1938) 309–319.
[42] D.L. Ou, P.D. Chevalier, I.A. Mackinnon, K. Eguchi, R. Boisvert, K. Su, Preparation of microporous ORMOSILs by thermal degradation of organically modified siloxane resin, J. Sol-Gel Sci. Technol. 26 (2003) 407–412.
[43] R. Nisticò, G. Magnacca, M. Antonietti, N. Fechler, Salted silica: sol-gel chemistry of silica under hypersaline conditions, Zeitschrift für Anorganische und Allgemeine Chemie 640 (2014) 582–587.
[44] R.J. Hunter, Principles and applications, in: Zeta Potential in Colloid Science, Academic Press, London UK, 1988.
[45] R. Nisticò, L.R. Celi, A. Bianco Prevot, L. Carlos, G. Magnacca, E. Zanzo, M. Martin, Sustainable magnet-responsive nanomaterials for the removal of

arsenic from contaminated water, J. Hazard. Mater. (2017), http://dx.doi.org/10.1016/j.jhazmat.2017.08.034.
[46] V. Bolis, G. Magnacca, G. Cerrato, C. Morterra, Microcalorimetric and IR-spectroscopic study of the room temperature adsorption of CO_2 on pure and sulphated t-ZrO_2, Thermochim. Acta 379 (2001) 147–161.
[47] V. Bolis, G. Cerrato, G. Magnacca, C. Morterra, Surface acidity of metal oxides. Combined microcalorimetric and IR-spectroscopic studies of variously dehydrated systems, Thermochim. Acta 312 (1998) 63–77.
[48] J. Kumirska, M. Czerwicka, Z. Kaczyński, A. Bychowska, K. Brzozowski, J. Thöming, P. Stepnowski, Application of spectroscopic methods for structural analysis of chitin and chitosan, Mar. Drugs 8 (2010) 1567–1636.
[49] B. Focher, A. Naggi, G. Torri, A. Cosani, M. Terbojevich, Structural differences between chitin polymorphs and their precipitates from solutions-evidence from CP-MAS ^{13}CNMR, FT-IR and FT-Raman spectroscopy, Carbohydr. Polym. 17 (1992) 97–102.
[50] H. Kaczmarek, J. Zawadzki, Chitosan pyrolysis and adsorption properties of chitosan and its carbonizate, Carbohydr. Res. 345 (2010) 941–947.
[51] G. Cárdenas, G. Cabrera, E. Taboada, S.P. Miranda, Chitin characterization by SEM, FTIR, XRD, and ^{13}C cross polarization/mass angle spinning NMR, J. Appl. Polym. Sci. 93 (2014) 1876–1885.
[52] A.K. Kercher, D.C. Nagle, Microstructural evolution during charcoal carbonization by X-ray diffraction analysis, Carbon 41 (2003) 15–27.
[53] S. Ifuku, T. Urakami, H. Izawa, M. Morimoto, H. Saimoto, Preparation of a protein–chitin nanofiber complex from crab shells and its application as a reinforcement filler or substrate for biomineralization, RSC Adv. 5 (2015) 64196–64201.
[54] M. Lawrinenko, D.A. Laird, Anion exchange capacity of biochar, Green Chem. 17 (2015) 4628–4636.
[55] G. Zheng, Q. Zhang, J.J. Cha, Y. Yang, W. Li, Z.W. She, Y. Cui, Amphiphilic surface modification of hollow carbon nanofibers for improved cycle life of lithium sulfur batteries, Nano Lett. 13 (2013) 1265–1270.
[56] R. Dominko, M.U.M. Patel, V. Lapornik, A. Vizintin, M. Kozelj, N.N. Tusar, I. Arcon, L. Stievano, G. Aquilanti, Analytical detection of polysulfides in the presence of adsorption additives by operand X-ray absorption spectroscopy, J. Phys. Chem. C 119 (2015) 19001–19010.
[57] M. Kavcic, K. Bucar, M. Petric, M. Zitnik, I. Arcon, R. Dominko, A. Vizintin, Operando resonant inelastic X-ray scattering: an appropriate tool to characterize sulfur in Li-S batteries, J. Phys. Chem. C 120 (2016) 24568–24576.